A comparison of fatigue-crack propagation behavior in sheet and plate aluminum–lithium alloys

K. T. Venkateswara Rao
Center for Advanced Materials, Lawrence Berkeley Laboratory and Department of Materials Science and Mineral Engineering, University of California at Berkeley, Berkeley, CA 94720 (U.S.A.)

R. J. Bucci
Alcoa Laboratories, Alcoa Center, Pittsburgh, PA 15069 (U.S.A.)

K. V. Jata
University of Dayton Research Institute, Dayton, OH 45469 (U.S.A.)

R. O. Ritchie
Center for Advanced Materials, Lawrence Berkeley Laboratory and Department of Materials Science and Mineral Engineering, University of California at Berkeley, Berkeley, CA 94720 (U.S.A.)

(Received September 17, 1990)

Abstract

The influence of wrought product form on the fatigue-crack propagation resistance of aluminum–lithium alloys was examined; specifically, results on the growth kinetics of long (greater than 10 mm) fatigue cracks in peak-aged Al–Li–Cu–Zr 2090-T8X and Al–Li–Cu–Mg–Zr 2091-T8 alloys, fabricated as sheet and plate, are presented as a function of microstructure, load ratio and specimen orientation. Contrary to popular belief, it was found that fatigue-crack growth rates at equivalent stress intensity levels are significantly faster and less dependent on specimen orientation in sheet than in plate. Such differences are attributed to the prominent role of crack-tip shielding during fatigue in these alloys, resulting from crack deflection and consequent crack closure from wedging of fracture-surface asperities, which microstructurally is related to variations in the degree of recrystallization, grain morphology and texture between the two product forms.

1. Introduction

Lithium-containing aluminum alloys constitute a new generation of low-density, high-strength and high-stiffness aerospace materials, aimed at replacing the 2000 and 7000 series aluminum alloys used in existing aircraft structures. Compared with traditional aluminum alloys, Al–Li alloys exhibit remarkably superior (long-crack) fatigue-crack propagation resistance [1–7]; in fact, at equivalent stress intensity levels, growth rates can be up to three orders of magnitude slower. This behavior was originally attributed to their higher elastic modulus and consequently lower crack-tip opening displacements, and to less accumulated crack-tip damage per cycle from a greater degree of reversible slip, due to marked planar-slip deformation arising from the shearable nature of coherent, ordered δ'-Al_3Li strengthening precipitates [1, 2]. More recent studies [3–7], however, have shown that their superior fatigue properties are principally associated with crack-tip shielding effects, induced in part from the strong planarity of slip. Crack-tip shielding mechanisms act to impede crack advance by lowering the local stress intensity actually experienced at the crack tip [8, 9]. Such mechanisms, which act principally in the crack wake, include transformation and microcrack toughening in ceramics, crack bridging in composites, and crack closure during fatigue-crack growth. In Al–Li alloys, such shielding occurs primarily from crack deflection and resulting

0921-5093/91/$3.50

(asperity-induced wedging) crack-closure mechanisms.

Such observations regarding the superior crack-growth resistance of Al–Li alloys mostly pertain to results for wrought thick-section plate, where microstructures are generally unrecrystallized, anisotropic and strongly textured, all factors which promote crack-path deflection and resultant crack closure in specific orientations. This is in part due to alloying additions of zirconium to form β'-Al_3Zr dispersoids, which inhibit recrystallization in hot-rolled plate (for thicknesses typically above 6 mm). However, the stability of the unrecrystallized structure is also dependent on product thickness during thermomechanical processing, such that in sheet material (*i.e.* thicknesses below about 4 mm), grain structures are partially or totally recrystallized and thus far more isotropic. It is in these microstructures that the superior fatigue-crack growth properties of Al–Li alloys may be compromised.

It is therefore the objective of the present paper to examine the influence of wrought-product form on the fatigue-crack propagation (long-crack) resistance of Al–Li alloys. Crack-growth behavior is examined in two Al–Li alloys: high-strength 2090-T8X, which has been cited as a replacement for the Al–Zn–Cu–Mg alloy 7075-T6, and low strength and high-toughness 2091-T8, which is a replacement for Al–Cu–Mg alloy 2024.

2. Materials and experimental procedures

Commercial Al–2.05Li–2.86Cu–0.12Zr (in weight per cent) alloy 2090 was processed at Alcoa using ingot-metallurgy techniques and rolled into 12.7 mm thick plate and 1.6 mm thin sheet. The products were then solution treated at 549 °C, cold-water quenched, and artificially aged at 163 °C to near peak-strength following a 3%–6% permanent stretch [5, 7]. Ageing practices differ slightly for plate and sheet products, and are designated as T81 and T83 respectively. Similarly, Al–1.7Li–1.99Cu–1.24Mg–0.12Zr (in weight per cent) alloy 2091 was fabricated as 12.7 mm thick plate and 1.6 mm thin sheet; the behavior was examined in an experimental, near peak-aged (T8) temper, obtained by additionally ageing the as-received, naturally aged (T351) material for 12 h at 135 °C. Ambient temperature mechanical properties are listed in Table 1.

TABLE 1

Room temperature mechanical properties (longitudinal orientation) of Al–Li alloys

	Yield strength (MPa)	UTS (MPa)	Percentage elongation (on 25 mm)	Fracture toughness[a] K_c (MPa $m^{1/2}$)
2090-T8X alloy				
12.7 mm T81 plate	552	589	9.3	36
1.6 mm T83 sheet	505	568	6.8	43
2091-T8 alloy				
12.7 mm plate	315	441	19.4	46
1.6 mm sheet	251	288	5.4	41

[a]L-T orientation.

As shown in Fig. 1(a), microstructures in 2090-T81 plate were coarse and unrecrystallized, with grains roughly 50 μm thick, 500 μm wide and elongated several millimeters in the rolling direction; similar unrecrystallized grain structures were apparent in 2091 plate (Fig. 1(c)). In contrast, grain morphologies in 2090-T83 sheet showed evidence for continuous recrystallization (20–30 μm equiaxed grains), similar to microstructures in 2091 sheet (Figs. 1(b), (d)). Deformation textures are seen in both sheet and plate alloys owing to prior cold-working processes, especially in the unrecrystallized microstructures [10–13]; they consist of both the hot rolling (Brass, S and Copper) and recrystallization (Cube and Goss) components of texture. Textural intensities, however, vary strongly with through-thickness location, particularly in plate alloys [11, 13]. As such, mechanical properties in Al–Li plate are highly anisotropic and vary with specimen orientation in the rolling plane and across the plate thickness [5, 7].

At the microscopic level, both 2090 plate and sheet products were hardened by coherent δ' spheres, θ'-like Al_2Cu and T_1 Al_2CuLi plates and β' dispersoids; a small degree of grain-boundary precipitation was also evident, which resulted in the formation of approximately 100 and 50 nm wide δ' precipitate-free zones (PFZs) in T83 sheet and T81 plate respectively [5, 7]. Conversely, peak-aged 2091 was hardened by a fine distribution of δ' particles and β' dispersoids in sheet and plate; no evidence of S Al_2CuMg laths was apparent [14, 15].

Fatigue-crack growth testing on long (greater than 10 mm) cracks was performed in moist, ambient air (22 °C, 45% relative humidity) environments using automated electro-servo-

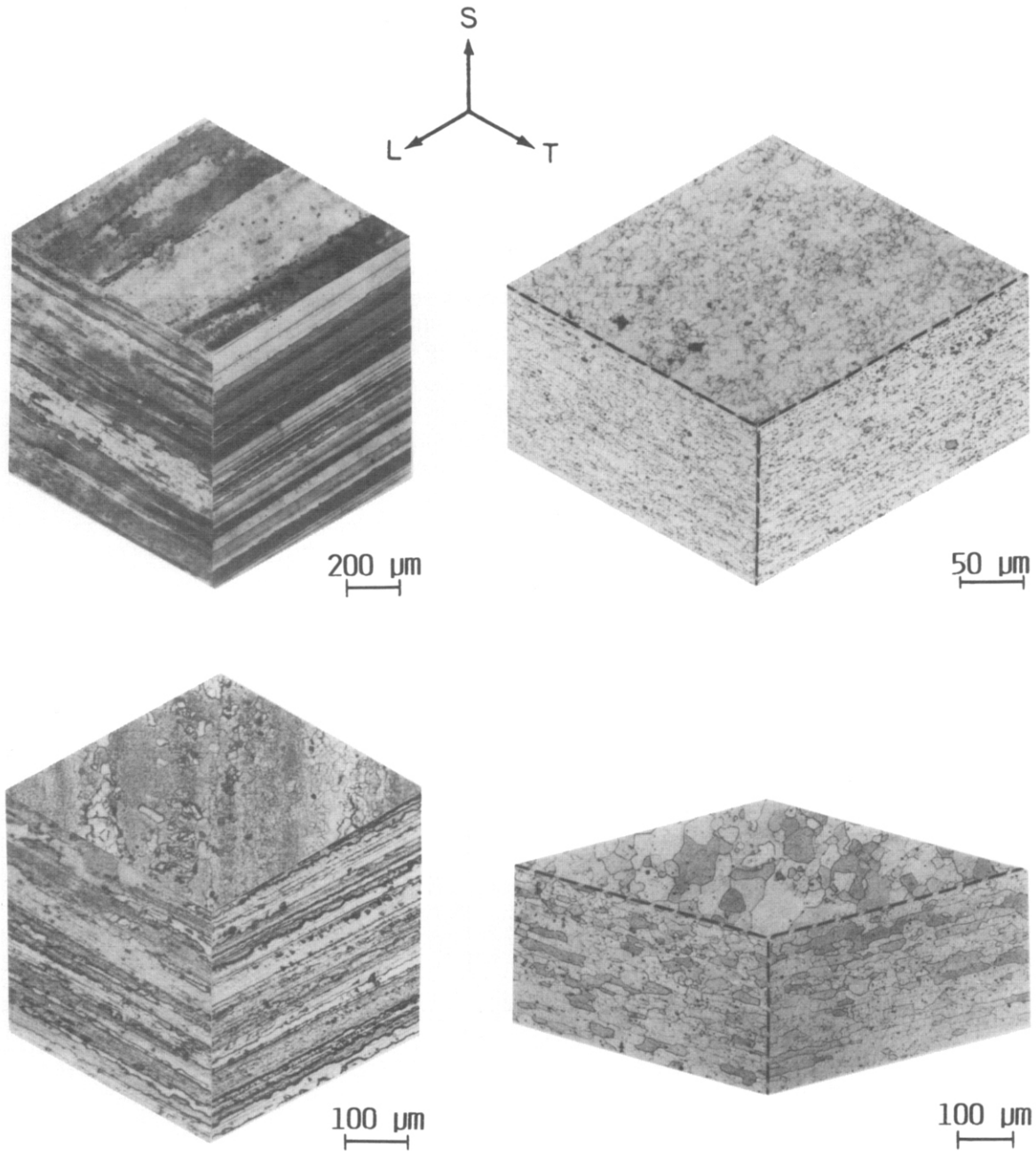

Fig. 1. Three-dimensional optical micrographs of grain structures (at mid-thickness $t/2$ locations) in (a) 12.7 mm 2090-T81 plate, (b) 1.6 mm 2090-T83 sheet, (c) 12.7 mm 2091-T8 plate and (d) 1.6 mm 2091-T8 sheet.

hydraulic testing machines operating under stress intensity K control, in general accordance with the ASTM Standard E647 [16]. Exponential load-shedding schemes, with a normalized K-gradient of $-0.1\ \mathrm{mm}^{-1}$, were used to measure crack-growth rates over a wide range of stress intensity levels ranging from instability K_{Ic} to the fatigue threshold ΔK_{TH}; the value of ΔK_{TH} was defined at a maximum growth rate of 10^{-12} m cycle^{-1}. 2090 and 2091 sheets were tested in their as-received full thickness, *i.e.* 1.6 mm, using compact-tension C(T) specimens; corresponding tests on plate material were conducted on 6.4 mm thick C(T) samples, machined at the mid-thickness ($t/2$) location. Specimens were tested in the L-T, T-L and L+45° orientations, at load ratios ($R = K_{min}/K_{max}$) of 0.10, 0.33 and 0.75 at a frequency of 50 Hz (sine wave). Crack length and

crack-closure levels were continuously monitored *in situ* using d.c. electrical potential and back-face strain compliance methods respectively [17]. Using the latter technique, the closure stress intensity K_{cl} defined at first contact of the mating fracture surfaces on unloading, was determined from the load corresponding to first deviation from linearity on the elastic-compliance curve.

Scanning electron microscopy was used to image fracture-surface morphologies. In addition, metallographic sections of the crack paths were examined optically, both perpendicular and parallel to the direction of crack growth; parallel profiles were taken at the specimen mid-thickness.

3. Results

3.1. Growth rate and crack-closure behavior

The variation in fatigue-crack propagation rates and corresponding crack-closure behavior of long cracks in peak-aged Al–Li–Cu–Zr 2090 and Al–Li–Cu–Mg–Zr 2091 alloys, fabricated as sheet and plate, are plotted in Figs. 2 and 3 as a function of the nominal stress intensity range, ΔK ($\Delta K = K_{max} - K_{min}$), at $R = 0.1$ for the L-T orientation; results in traditional 7075-T6 products are also shown for comparison. Several points are worthy of note. First, fatigue cracks in both Al–Li alloys grow up to 2–3 orders of magnitude faster in sheet compared with plate, particularly in 2090 at ΔK levels approaching the fatigue threshold; in 2091, differences are most apparent above ΔK levels of 6 MPa $m^{1/2}$. In contrast, the 7075-T6 alloy shows no such differences between sheet and plate, at least for ΔK levels below 20 MPa $m^{1/2}$. Second, the faster crack-growth rates measured in both 2090 and 2091 sheet are consistent with lower measured crack-closure levels in sheet contrasted with closure levels in plate. Third, both 2090 and 2091 alloy sheet display generally equal or superior fatigue-crack

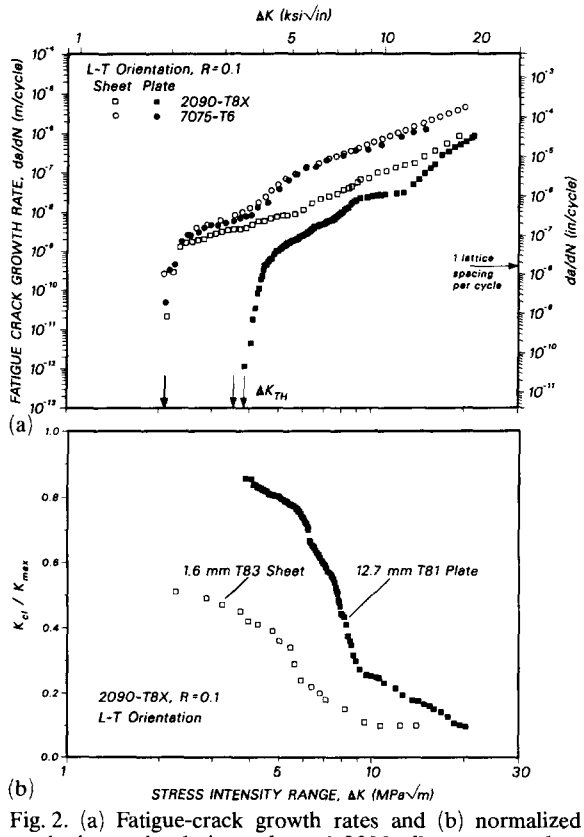

Fig. 2. (a) Fatigue-crack growth rates and (b) normalized crack-closure levels in peak-aged 2090 alloy processed as T83 sheet and T81 plate, in the L-T orientation at $R = 0.1$, as a function of nominal stress intensity range ΔK. Growth-rate data are compared with corresponding results on 7075-T6 alloys [7, 18]. Results on 12.7 mm thick plate were obtained using 6.4 mm thick specimens machined from the $t/2$ location.

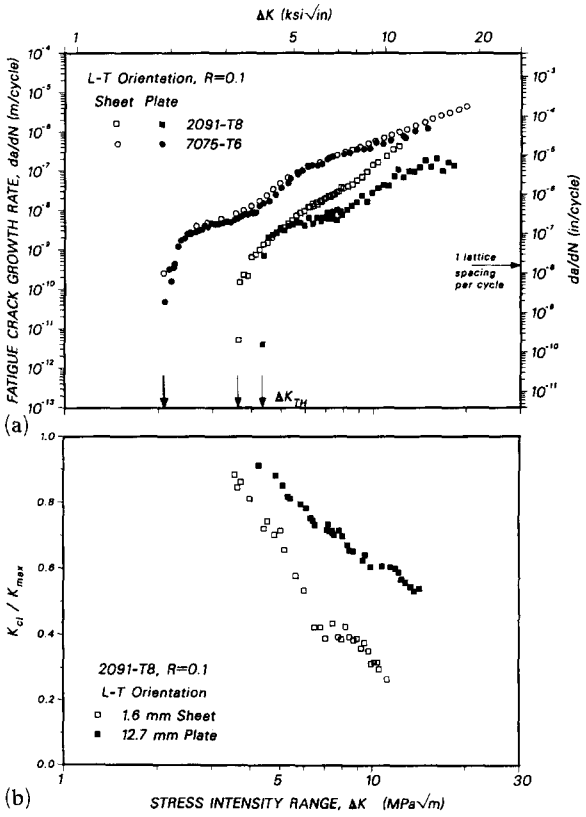

Fig. 3. (a) Fatigue-crack growth rates and (b) normalized crack-closure levels in 2091-T8 sheet and plate, in the L-T orientation at $R = 0.1$, as a function of nominal stress intensity range ΔK. Growth-rate data are compared with corresponding results on 7075-T6 alloys [7, 18]. Results on 12.7 mm thick plate were obtained using 6.4 mm thick specimens machined from the $t/2$ location.

growth resistance than the corresponding 7075-T6 alloys.

The higher growth rates and lower closure levels in 2090-T83 sheet are associated with essentially linear crack-path morphologies in the direction of crack growth (Fig. 4(a)) and with planar crack fronts through the thickness (Fig. 4(c)), resulting in relatively flat fracture surfaces (Fig. 4(e)). Conversely, the 2090-T81 plate material exhibits highly deflected and meandering crack profiles, both along the crack-growth direction and across the specimen thickness (Figs. 4(b), (d)), consistent with much higher closure levels from crack wedging by enlarged fracture-

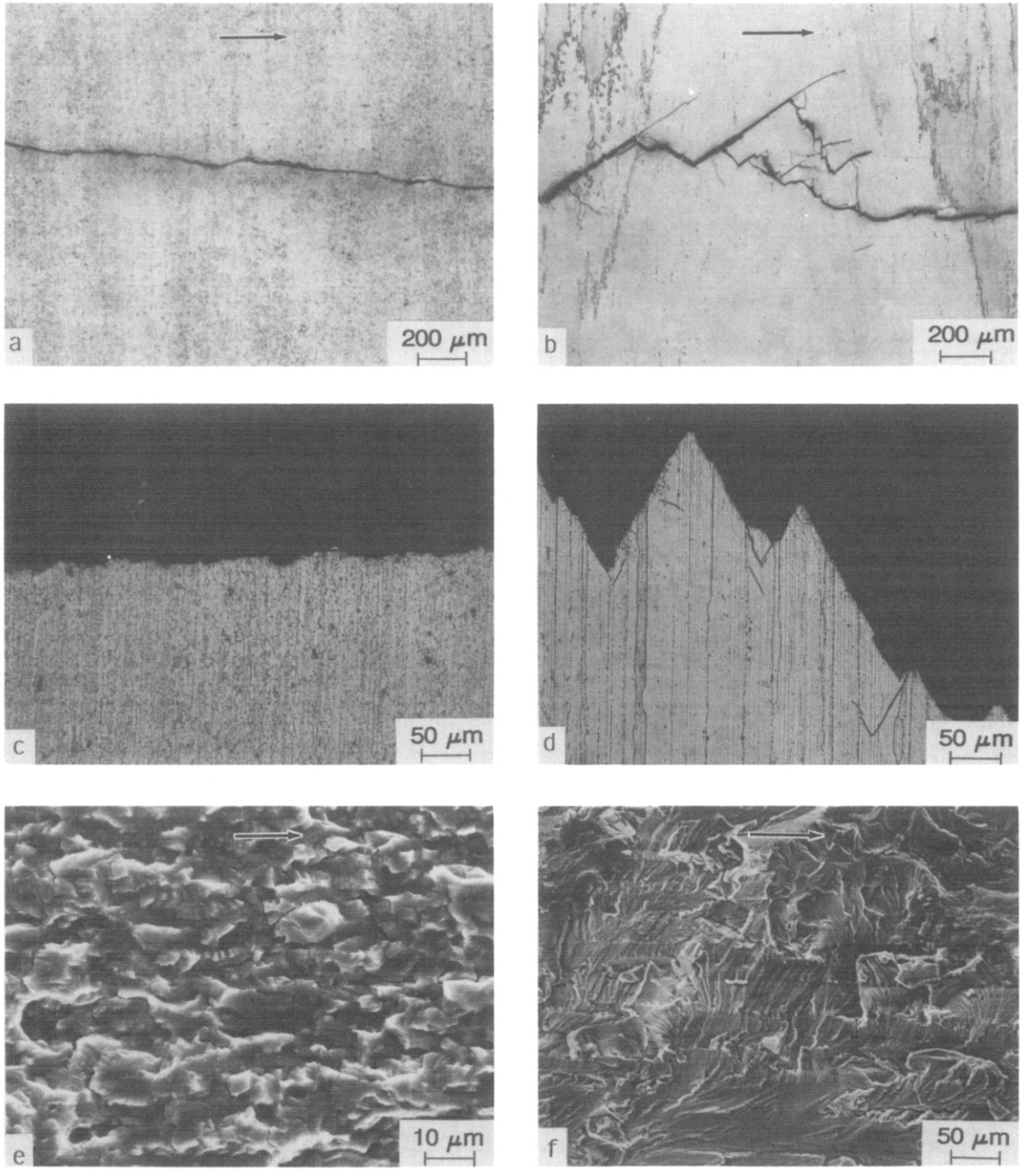

Fig. 4. Comparison of fatigue-crack path and fracture-surface morphologies in 2090 alloy processed as T83 sheet (left) and T81 plate (right), showing (a), (b) crack paths along the crack-growth direction, (c), (d) crack profiles across the specimen thickness and (e), (f) fracture surfaces. Arrows indicate the general direction of crack growth.

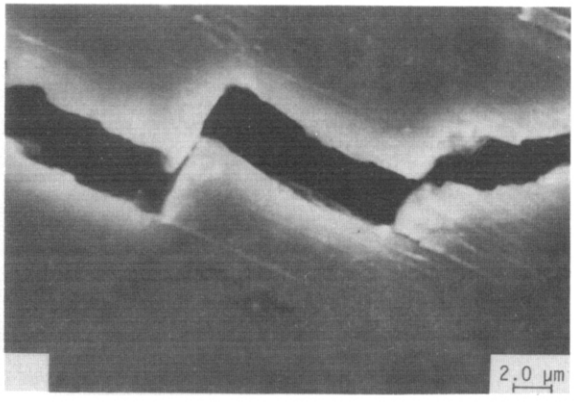

Fig. 5. Example of asperity-induced wedging of fatigue-fracture surfaces in Al–Li alloy plate, caused by faceted crack extension along slip bands. The micrograph was obtained by imaging the specimen surface of 12.7 mm thick 2090-T81 plate sample at $\Delta K = 8$ MPa $m^{1/2}$, using scanning electron microscopy. Arrow indicates the general direction of crack advance.

surface asperities (roughness-induced crack closure) (Fig. 5). Such crack advance proceeds along {111} slip bands [6, 10], owing to the shearable, coherent δ' precipitates and pronounced texture in plate material, resulting in an unusually rough fracture-surface topography covered with large transgranular shear facets (Fig. 4(f)). Similar differences may be noted between sheet and plate in the 2091 alloy, although they are less pronounced (Fig. 6). In both product forms, however, no distinct transition in fracture mechanism or evidence of intergranular delamination across the specimen thickness was observed over the spectrum of growth rates investigated.

3.2. Effect of load ratio

The influence of load ratio on fatigue-crack growth rates in 2090-T83 sheet and 2090-T81 plate is shown in Fig. 7. Similar to most I/M alloys, higher load ratios induce faster crack velocities, particularly at near-threshold stress intensity levels. The magnitude of the effect, however, is more pronounced in the plate material where closure levels are high at $R = 0.1$, owing to asperity-induced crack wedging. With increasing R, the larger crack-tip opening displacements act to diminish the shielding from crack wedging, such that differences in crack-growth behavior between sheet and plate become less apparent.

3.3. Effect of specimen orientation

Crack-growth behavior in Al–Li alloy plate is also highly anisotropic, which is again a consequence of the differing crack-path morphologies with specimen orientation. In fact, in the L-T, T-L and L+45° orientations (in the rolling plane) in 2090-T8, growth rates at a given ΔK can vary by up to three orders of magnitude (Fig. 8(a)). The more commonly tested L-T and T-L orientations exhibit the slowest growth rates; the L+45° specimens, oriented at 45° to the principal rolling direction, show the fastest. In addition, growth rates in the in-plane orientations (L-T, T-L) for thick section plates have been found to vary with specimen location through the plate thickness [6, 7, 13]. However, crack-growth rates are less dependent on orientation in the sheet material, where the contribution from crack closure is smaller (Fig. 8(b)).

4. Discussion

Explanations proposed in the literature [19–25] to account for the effect of specimen thickness on fatigue-crack propagation in metallic materials are generally conflicting; in fact, increasing the thickness has been found to accelerate, retard or have no effect on crack advance. Differences in behavior have been attributed to variations in fracture mode (mode I *vs.* II or III), stress state (plane stress *vs.* plane strain), the onset of general yielding and resulting change in fracture mechanisms and crack-closure effects. For example, higher growth rates observed in thick sections can be due to inherently faster crack advance under plane-strain conditions, induced by lower (plasticity-induced) crack-closure levels [19–22] and an increasing contribution to crack advance from fast-fracture (static) modes [23, 24] triggered by the triaxial stress state. Conversely, rapid crack extension in thin sheet may be induced by larger plastic zone and specimen-geometry effects [23, 25], which promote stress relaxation and the early onset of approximately 45° slant fracture. The role of crack-divider delamination toughening, which has significant influence on the cryogenic fracture-toughness behavior of Al–Li alloys [26], is also presumed minimal owing to the lack of through-thickness splitting in these alloys during fatigue-crack propagation. These explanations, however, pertain more to high growth rates approaching instability; they are less important at

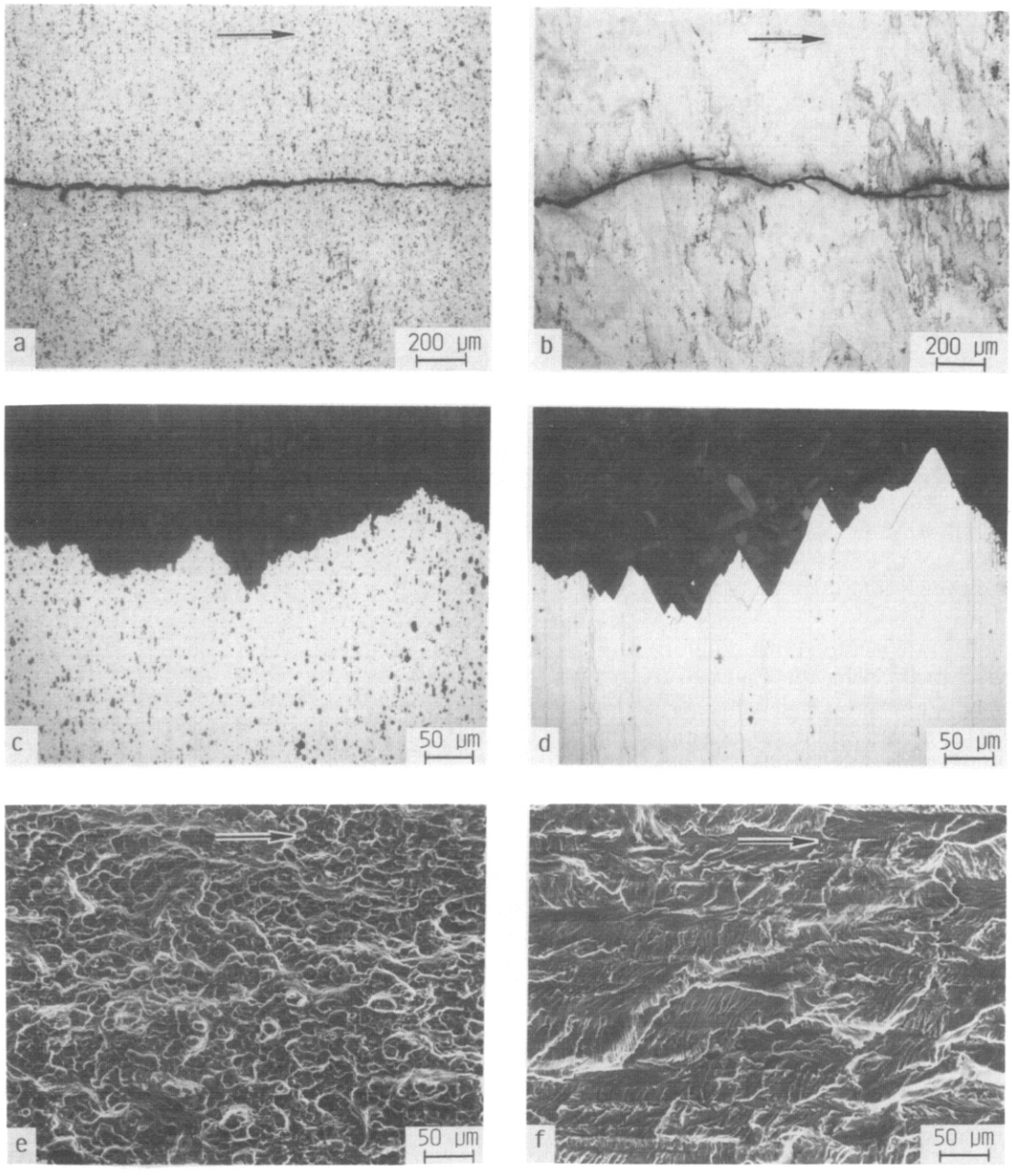

Fig. 6. Comparison of fatigue-crack path and fracture-surface morphologies in 2091-T8 sheet (left) and plate (right), showing (a), (b) crack paths along the crack-growth direction, (c), (d) crack profiles across the specimen thickness and (e), (f) fracture surfaces. Arrows indicate general direction of crack growth.

lower ΔK levels where crack-tip deformation conditions generally approach plane strain for most thicknesses.

Observations in the current work are inconsistent with these explanations to account for the influence of thickness on fatigue-crack propagation. For example, crack growth in the Al–Li alloy sheet and plate examined occurs predominantly under plane-strain conditions below stress intensity levels of 10 MPa $m^{1/2}$ (maximum plastic-zone sizes (approximately $1/2\pi\{K_{max}/\sigma_y\}^2$) and shear-lip sizes at $\Delta K = 15$ MPa $m^{1/2}$ are at least less than 10% of the specimen thickness). Moreover, no evidence of fast-fracture modes was apparent over the entire spectrum of crack-growth rates; a flat (square) mode and transgranular shear fracture mechanism prevail at all stress intensities. However, it is clear that crack-closure levels are

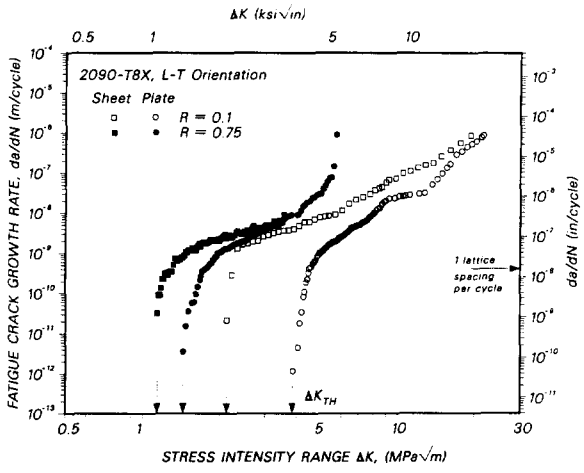

Fig. 7. Influence of load ratio R on fatigue-crack propagation rates in peak-aged 2090-T38 sheet and T81 plate material.

significantly higher in the thick plate than in the thin sheet alloys.

Accordingly, it is concluded that differences in fatigue-crack growth behavior between Al–Li sheet and plate alloys are principally associated with microstructurally induced variations in crack-path deflection and resulting roughness-induced crack closure from the wedging of fracture-surface asperities [3–6]. For both plate alloys, the planar nature of slip (due to coherent δ'-particle hardening) results in faceted crack growth along slip bands, which promotes periodic deflection in the crack-growth direction (Figs. 4(b), 6(b)). In addition, pronounced deformation texture promotes crystallographic crack-path tortuosity across the specimen thickness (Figs. 4(d), 6(d)); the sharp facets, with an included angle of 60° have been shown to be traces of {111} slip planes [10]. These effects, combined with the coarser, unrecrystallized and elongated grain structures in thick plate, provide the principal sources of high shielding levels, which result in slower crack-propagation rates. In contrast, shielding effects are less prominent in sheet alloys (Figs. 2(b), 3(b)) where the finer, recrystallized and equiaxed grain structures induce more linear crack paths (Figs. 4(a), 6(a)); this diminishes closure effects and results in faster crack-growth rates. Consistent with these explanations, crack-growth kinetics even in thick plates are reported to be accelerated on the near-surface regions of plate, where the grain structures are partially recrystallized and less textured, compared with

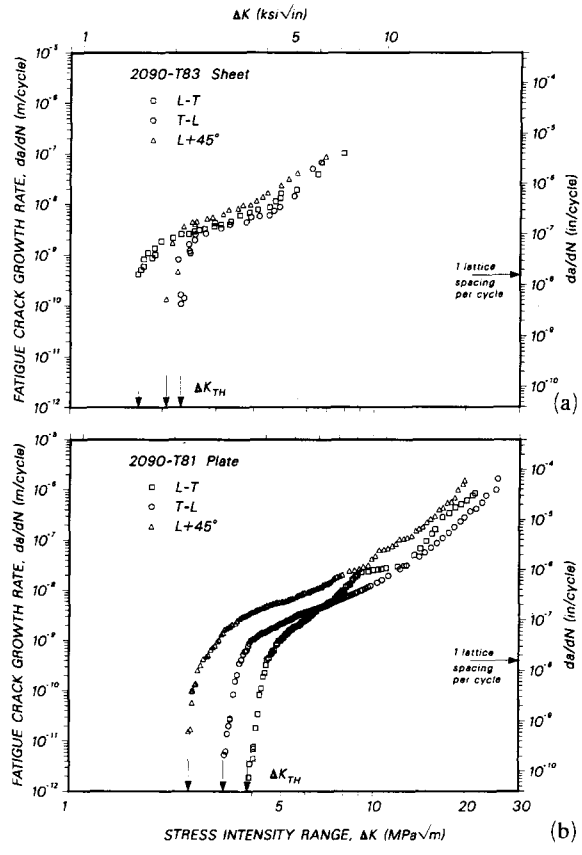

Fig. 8. Effect of specimen orientation in the rolling plane on the fatigue-crack propagation rates in Al–Li alloy 2090 processed as (a) 1.6 mm T83 sheet ($R = 0.33$) and (b) 12.7 mm T81 plate ($R = 0.1$, $t/2$ location).

the highly anisotropic and textured microstructures at the mid-thickness location [13].

The closure contribution is similarly responsible for the fact that differences in growth-rate behavior between sheet and plate alloys become less apparent at high load ratios (Fig. 7), as the higher mean stresses act to limit crack wedging because the crack faces remain apart for a larger portion of the loading cycle. However, growth rates in 2090-T83 sheet exceed those in T81 plate even at $R = 0.75$, because the near-threshold closure stress intensity K_{cl} values in plate exceed 0.85 of K_{max}; R ratios above 0.85 are therefore needed to suppress totally roughness-induced closure effects in plate alloys. Similarly, as the crack-growth behavior in recrystallized sheet is less dependent on crack-path geometry than in plate, the variation in growth rates with specimen orientation is correspondingly less evident [27] (Fig. 8(a)).

We thus conclude that thickness effects on fatigue-crack growth in Al–Li alloy product forms can be attributed to variations in roughness-induced crack closure caused by intrinsic microstructural changes during thermomechanical processing. Specifically, recrystallization is suppressed in thick-section plate owing to the presence of β' dispersoids; grain structures are therefore coarse, highly anisotropic and textured, thereby promoting inhomogeneous (planar) slip. The consequent crack-path deflection and resulting crack closure lead to excellent crack-growth resistance in the plate Al–Li alloys, albeit confined to long (greater than 10 mm) through-thickness cracks in specific orientations [5, 6]. Such properties, however, are compromised somewhat in sheet alloys as recrystallization occurs more readily during hot rolling owing to greater heat losses (higher surface area to volume ratio). Overall, despite a diminished role of closure, the Al–Li alloy sheet still displays crack-growth resistance superior to that of many traditional aluminum alloys (*e.g.* 7075), presumably owing to the higher modulus and enhanced slip reversibility associated with coherent-particle hardening in the Al–Li alloy system.

5. Conclusions

Based on a study on fatigue-crack propagation behavior of long (greater than 10 mm) cracks in peak-aged Al–Li–Cu–Zr 2090-T8X and Al–Li–Cu–Mg–Zr 2091-T8 alloys, processed as 1.6 mm thin sheet and 12.7 mm thick plate, the following conclusions can be made.

(1) Rates of fatigue-crack propagation in both Al–Li alloys, at a load ratio of $R = 0.1$, are found to be up to 2–3 orders of magnitude faster in sheet compared with plate at equivalent stress intensity levels. No such differences between sheet and plate are observed for traditional 7075-T6 aluminum alloys.

(2) Fatigue-crack growth rates in 2090-T83 sheet are less sensitive to load ratio and specimen orientation (in the rolling plane) compared with 2090-T81 plate. The influence of product form on crack-growth rates is thus less pronounced at high load ratios ($R = 0.75$).

(3) Such differences in growth-rate behavior are attributed primarily to microstructurally induced variations in crack-tip shielding. In thick plate, where microstructures remain predominantly unrecrystallized with coarse elongated grains and strong deformation texture, fatigue-crack paths are unusually tortuous; such morphology promotes marked (roughness-induced) crack closure, concomitant with reduced growth rates. Conversely, the sheet microstructures are recrystallized with a fine relatively equiaxed grain size; crack paths are correspondingly far more linear leading to lower closure levels and faster growth rates.

(4) Despite the higher crack-growth rates observed in Al–Li alloys sheet, both 2090-T8 and 2091-T8 sheet alloy still display superior fatigue-crack growth resistance compared with traditional 7075-T6 aluminum alloys.

Acknowledgments

This work was supported by the Director, Office of Energy Research, Office of Basic Energy Sciences, Materials Sciences Division of the U.S. Department of Energy under Contract No. DE-ACO3-76SF00098 (KTVR and ROR), by the Department of the Navy, Naval Surface Warfare Center, under Contract No. N60921-84-C-0078 (RJB) and the U.S. Air Force Contract No. F33615-88-C-5437 (KVJ).

References

1 E. J. Coyne, T. H. Sanders and E. A. Starke, in T. H. Sanders and E. A. Starke (eds.), *Aluminum–Lithium Alloys*, TMS-AIME, Warrendale, PA, 1981, p. 293.
2 S. J. Harris, B. Noble and K. Dinsdale, in T. H. Sanders and E. A. Starke (eds.), *Aluminum–Lithium Alloys II*, TMS-AIME, Warrendale, PA, 1983, p. 219.
3 A. K. Vasudévan, P. E. Bretz, A. C. Miller and S. Suresh, *Mater. Sci. Eng., 64* (1984) 113.
4 K. V. Jata and E. A. Starke, *Metall. Trans. A, 17* (1986) 1011.
5 K. T. Venkateswara Rao, W. Yu and R. O. Ritchie, *Metall. Trans. A, 19* (1988) 549.
6 K. T. Venkateswara Rao, R. S. Piascik, R. P. Gangloff and R. O. Ritchie, in T. H. Sanders and E. A. Starke (eds.), *Aluminum–Lithium Alloys*, Vol. II, MACE Publications, Birmingham, 1989, p. 955.
7 R. J. Bucci, R. C. Malcolm, E. L. Colvin, S. Murtha and R. S. James, *Final Report, Contract N60921-84-C-0078, Tech. Rep. NSWC TR 89-106*, 1989 (Naval Surface Warfare Center, Silver Spring, MD).
8 R. O. Ritchie, *Mater. Sci. Eng. A, 103* (1988) 15.
9 A. G. Evans, in R. P. Wei and R. P. Gangloff (eds.), *Fracture Mechanics: Perspectives and Directions (20th Symp.), ASTM STP 1020*, ASTM, Philadelphia, PA, 1989, p. 267.
10 G. R. Yoder, P. S. Pao, M. A. Imam and L. A. Cooley, *Scripta Metall., 22* (1988) 1241.
11 A. K. Vasudévan, W. G. Fricke, R. C. Malcolm, R. J. Bucci, M. A. Przystupa and F. Barlat, *Metall. Trans. A, 19* (1988) 731.

12 C. J. Warren and R. J. Rioja, in T. H. Sanders and E. A. Starke (eds.), *Aluminum–Lithium Alloys*, Vol. I, MACE Publications, Birmingham, 1989, p. 417.
13 P. S. Pao, L. A. Cooley, M. A. Imam and G. R. Yoder, *Scripta Metall., 23* (1989) 1455.
14 R. De Jesus and A. J. Ardell, in T. H. Sanders and E. A. Starke (eds.), *Aluminum–Lithium Alloys*, Vol. II, MACE Publications, Birmingham, 1989, p. 661.
15 A. F. Smith, *Mater. Sci. Technol., 5* (1989) 533.
16 ASTM Standard E 647-88a, *1989 Annual Book of ASTM Standards*, Vol. 3.01, ASTM, Philadelphia, PA, 1989, p. 646.
17 R. O. Ritchie and W. Yu, in R. O. Ritchie and J. Lankford (eds.), *Short Fatigue Cracks*, TMS-AIME, Warrendale, PA, 1986, p. 167.
18 P. E. Bretz, A. K. Vasudévan, R. J. Bucci and R. C. Malcolm, *Final Report, Contract N00019-79-C-0258*, 1981 (Naval Air Systems Command, Washington, DC).
19 T. C. Lindley and C. E. Richards, *Mater. Sci. Eng., 14* (1974) 281.
20 J. Schijve, *Eng. Fract. Mech., 11* (1979) 182.
21 A. J. McEvily, *Met. Sci., 11* (1977) 274.
22 R. O. Ritchie, W. Yu, A. F. Blom and D. K. Holm, *Fat. Fract. Eng. Mater. Struct., 10* (1987) 343.
23 R. O. Ritchie, R. F. Smith and J. F. Knott, *Met. Sci., 9* (1975) 485.
24 J. R. Griffiths and C. E. Richards, *Mater. Sci. Eng., 11* (1973) 305.
25 A. R. Jack and A. T. Price, *Acta Metall., 20* (1972) 857.
26 K. T. Venkateswara Rao, W. Yu and R. O. Ritchie, *Metall. Trans. A, 20* (1989) 485.
27 K. V. Jata and J. Ruschau, in E. W. Lee, E. H. Chia and N. J. Kim (eds.), *Light-Weight Alloys for Aerospace Applications*, TMS-AIME, Warrendale, PA, 1989, p. 195.